Artificial Intelligence 301 (2021) 103560

Contents lists available at ScienceDirect

Artificial Intelligence

www.elsevier.com/locate/artint

Path-length analysis for grid-based path planning

James P. Bailey [a,*], Alex Nash, Craig A. Tovey [b], Sven Koenig [c]

[a] Texas A&M University, United States of America
[b] Georgia Institute of Technology, United States of America
[c] University of Southern California, United States of America

ARTICLE INFO

Article history:
Received 21 February 2020
Received in revised form 15 July 2021
Accepted 20 July 2021
Available online 27 July 2021

Keywords:
Path planning
Any angle path planning
Robotics
Search
Computational geometry

ABSTRACT

In video games and robotics, one often discretizes a continuous 2D environment into a regular grid with blocked and unblocked cells and then finds shortest paths for the agents on the resulting grid graph. Shortest grid paths, of course, are not necessarily true shortest paths in the continuous 2D environment. In this article, we therefore study how much longer a shortest grid path can be than a corresponding true shortest path on all regular grids with blocked and unblocked cells that tessellate continuous 2D environments. We study 5 different vertex connectivities that result from both different tessellations and different definitions of the neighbors of a vertex. Our path-length analysis yields either tight or asymptotically tight worst-case bounds in a unified framework. Our results show that the percentage by which a shortest grid path can be longer than a corresponding true shortest path decreases as the vertex connectivity increases. Our path-length analysis is topical because it determines the largest path-length reduction possible for any-angle path-planning algorithms (and thus their benefit), a class of path-planning algorithms in artificial intelligence and robotics that has become popular.

Published by Elsevier B.V.

1. Introduction

Agents, such as game characters and robots, navigate in continuous 2D environments and thus have to find paths. They often discretize their environments into regular grids whose cells are equilateral and equiangular polygons. Some of these polygons can be blocked. For example, robots use evidence grids [1] or, synonymously, occupancy grids to keep track of the locations of obstacles. Video games and robots also use grids as maps and might associate information with polygons, such as the type of terrain, hidden objects or weather information. For example, the video game "Company of Heroes" and the Mars rovers Spirit and Opportunity [2] use 2D square grids. But other kinds of grids are used as well, especially in video games. For example, the video game "Civilization VI" uses 2D hexagonal grids, as shown in Fig. 1. One advantage of 2D hexagonal grids over 2D square grids is that paths can often be found faster on 2D hexagonal grids than 2D square grids, as has been shown both analytically [3] and experimentally [4].

The agents then find shortest grid paths (SGPs) on the grid graphs constructed from the grids and move along them [5,3,6]. These paths need to be unblocked, that is, are not allowed to pass through the interior of blocked polygons or between blocked polygons that share a side. SGPs, of course, are not necessarily true shortest paths (TSPs) in the continuous 2D environments. In this article, we therefore study how much longer an SGP can be than a corresponding TSP.

* Corresponding author.
E-mail addresses: jamespbailey@tamu.edu (J.P. Bailey), alexwnash@gmail.com (A. Nash), cat@gatech.edu (C.A. Tovey), skoenig@usc.edu (S. Koenig).

https://doi.org/10.1016/j.artint.2021.103560
0004-3702/Published by Elsevier B.V.

Fig. 1. Screen Shot of the Video Game "Civilization VI" by Firaxis Games.

Significance: SGPs can often be found faster than the corresponding TSPs, but are also typically longer which results in larger navigation times and fuel consumptions. Path planning on visibility graphs [7,8], for example, finds TSPs in continuous 2D environments, but is often slow since the number of edges can grow quadratically in the number of vertices [9]. Path planning on grids, on the other hand, often finds longer paths, but is fast since the vertex connectivity does not depend on the number of vertices. Understanding this trade-off between the planning time and the length of the resulting path allows practitioners to choose appropriate path-planning algorithms for their applications. We analyze how much longer an SGP is than a corresponding TSP to help characterize this trade-off. Our path-length analysis complements other studies of the planning times for the tessellations that we study in this article or the path lengths for other tessellations. For example, researchers have analyzed how much longer a SGP formed by the edges of Delaunay triangulations without blocked polygons is than a corresponding TSP [10,11]. For the 2D square tessellation, upper bounds parameterized in k have been given on how much longer than the TSP path the SGP may need to be when: the set of edges is augmented to be those passing through at most k rows and k columns [12]; the set of edges is augmented by setting the vertex degree to 2^k [13].

Our path-length analysis is topical because it determines the largest path-length reduction possible for any-angle path-planning algorithms [14] (and thus their benefit), a class of path-planning algorithms in artificial intelligence and robotics that has become popular. Any-angle path-planning algorithms are often based on A* [15] and propagate information along grid edges (like A*, to be fast) without constraining the resulting paths to grid edges (unlike A*, to find shorter paths than SGPs) [14]. Some any-angle path-planning algorithms, such as Anya [16], even find TSPs in continuous 2D environments. Some any-angle path-planning algorithms have been proposed in the context of video games [17–19]. Examples are Block A* [20], Anya, Theta* [21] and Lazy Theta* [22] and a chapter in a game-programming book [18]. Other any-angle path-planning algorithms have been proposed in the context of robotics. An example is Field D*, which has been used on various robots – including the Mars rovers Spirit, Opportunity and Curiosity [2,23]. Researchers have also proposed to use Field D* on unmanned underwater vehicles [24] as well as Theta*, Lazy Theta*, and Accelerated A* [25] on unmanned aerial vehicles [26–28], for example to avoid collisions or bad weather. Any-angle path-planning algorithms can operate on various kinds of grid graphs. For example, Field D* [29] was initially designed for 2D square grids but has been extended to 3D cubic grids [30] and a variety of other graph topologies [31,32], and Theta* [33] and Lazy Theta* [34] were designed to operate on arbitrary Euclidean graphs. See [14] for an overview on any-angle path-planning algorithms.

We consider all regular grids with any arrangement of blocked polygons that tessellate continuous 2D environments (namely, grids with SQUAREs, TRIangles, and HEXagons as polygons). We transform them into grid graphs by placing vertices at the corners of the polygons. Placing vertices at the corners rather than the centers of 2D square grids typically results in shorter paths since TSPs in 2D grids change their headings only at the corners, as has been shown both analytically and experimentally [35], and is thus often done by any-angle path-planning algorithms. The closed-form interpolation equation of Field D*, for example, requires vertices to be placed there. We study 5 different vertex connectivities that result from both different tessellations and different definitions of the neighbors of a vertex, resulting in 6-Tri, 4-Square, 8-Square, 3-Hex, and 12-Hex grid graphs, where the integer indicates the vertex connectivity. For example, a vertex in 4-Square (or 8-Square) grid graphs connects to its neighbors in the 4 (or 8, respectively) compass directions if the straight-line paths between them are unblocked.

Assumptions: We assume, as is often done for theoretical analyses, that the agents are omnidirectional points and each polygon has a traversal cost per unit of distance traveled of either one or, if it is blocked, infinity. Thus, our path-

Table 1
Worst-Case Ratios Between Shortest Grid Paths (SGPs) and True Shortest Paths (TSPs).

Polygons	Vertex Connectivity	SGP can be up to % Longer than TSP	
Triangles	6	$100 \cdot \frac{2}{\sqrt{3}} \approx 115.47$	(tight)
Squares	4	$100 \cdot \sqrt{2} \approx 141.42$	(tight)
	8	$100 \cdot \frac{2}{\sqrt{2+\sqrt{2}}} \approx 108.24$	(asymptotically tight)
Hexagons	3	$100 \cdot \frac{3}{2} = 150$	(tight)
	12	$100 \cdot (\sqrt{6} - \sqrt{2}) \approx 103.53$	(asymptotically tight)

length analysis only approximates reality where agents often have both extent and kino-dynamic motion constraints and environments contain obstacles of more complex shapes. Agents would then first grow the obstacles sufficiently, next cover them with blocked polygons, plan their paths, and finally use controllers that take their motion constraints into account and stay close to the resulting paths.

Contributions: Our path-length analysis yields worst-case ratios of the lengths of an SGP and a corresponding TSP in a unified framework for all regular tessellations of continuous 2D environments, where only 3-Hex grid graphs need to be treated slightly differently since they have properties different from the other grid graphs. For example, an SGP typically moves in at most 2 different directions on 2D grid graphs but can move in 3 different directions on 3-Hex grid graphs. The worst-case ratios determine how much longer at most is an SGP than is a corresponding TSP over all path-planning instances. Our path-length analysis generalizes existing results on the worst-case ratios for 8-Square grid graphs [29] and 6-Hex grid graphs [36]. These previous path-length analyses are specific to particular vertex connectivities and ignore the potential effects of blocked polygons. For example, it is known that an SGP for 8-Square grid graphs without blocked polygons can be about 8 percent longer than a corresponding TSP but not longer [29], which raises the question whether this percentage can be larger in the presence of blocked polygons. We show that this is not possible. Our path-length analysis in this article also substantially improves on our own previous path-length analysis [9], which makes extensive use of case enumeration and is thus long and inelegant. The prior work analyzes fewer vertex connectivities (but also cases where vertices are placed at the centers of the polygons).

Results: Table 1 summarizes the worst-case ratios of the lengths of an SGP and a corresponding TSP. All worst-case ratios are either tight (that is, can be attained for some path-planning instance) or asymptotically tight (an arbitrarily close ratio can be attained). They decrease as the vertex connectivity increases. Interestingly however, we show that when the TSP consists of a single line segment, as is the case when there are no blocked polygons, the worst-case ratio for 3-Hex converges to 4/3 as the TSP grows large. Thus, if the grid path consists of long line segments, the worst-case performance of 3-Hex is actually better than the worst-case performance of 4-Square. See [14] for a high-level overview of a subset of these and other results.

Structure: We define our terminology and notation in Section 2. We show that without loss of generality we may assume the starting and ending locations (s and t) have line of sight – i.e., the segment $\overline{st}$ avoids blocked polygons – whenever looking for the worst-case ratio between the lengths of an SGP and TSP (Theorem 1). In Section 3, we determine the worst-case ratio for the 8-Square grid graph. Specifically, we characterize the directions used in a SGP (Theorem 2) and show that blocked squares have no impact on the SGP when there is line of sight between s and t (Theorem 3). Finally, we prove the worst-case ratio and demonstrate that it is asymptotically tight. In Section 4, we then provide a set of properties that allow us to extend the proofs for the 8-Square grid graph to a larger family of grid graphs including 4-Square, 6-Tri, and 12-Hex. We then calculate the worst-case ratios and prove tightness for 4-Square, 6-Tri, and 12-Hex grid graphs. In Section 5, we show that the structure of 3-Hex grid graphs is fundamentally different and perform a separate analysis on it.

2. Notation and definitions

In this paper, we consider grid graphs induced by tessellations of $\mathbb{R}^2$ by regular polygons (triangles, squares, and hexagons) with unit side length. For simplicity, we arrange the tessellation so that one side of each polygon is parallel to the horizontal axis and so that there is a polygon with a vertex (corner point) at the point $(0, 0)$. Grid paths are formed by moving from vertex to vertex of the polygons tessellating the plane while using some set of allowed movements. Most commonly, grid paths are allowed to move along the edge of a polygon. When tessellating $\mathbb{R}^2$ by squares, this corresponds to either moving in one of the 4-cardinal directions, e.g., north. We denote this type of grid graph as a *4-Square* grid graph. Another common selection is to allow grid paths to move to any vertex within the same polygon. With a square tessellation, this allows movement in the 4-intercardinal directions, e.g., north-east, in addition to the 4-cardinal directions. We denote this type of grid graph as an *8-Square* grid graph. Both square grid graphs and their allowed movements are depicted in Fig. 2

Unpassable terrain is represented by blocked polygons – a subset of the polygons tessellating the plane – and every path must avoid them. A path *avoids* a blocked polygon if every part of the path intersects with an unblocked polygon. We remark that this definition allows a path to squeeze through two diagonally adjacent blocked polygons as depicted in Fig. 3, which may be undesirable in some settings. Fortunately, we show that traveling through diagonally adjacent blocked

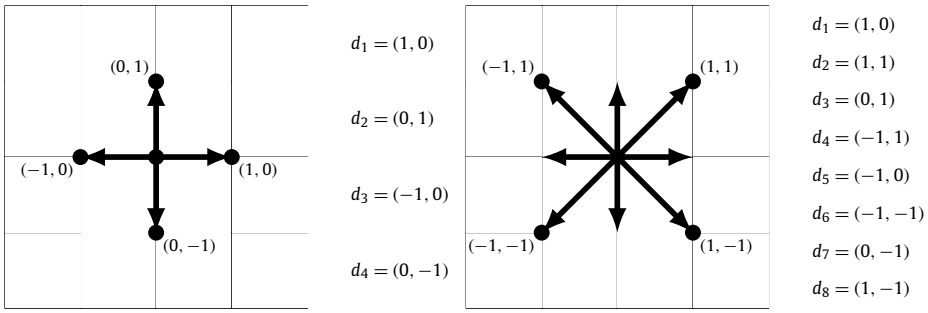

Fig. 2. Movements allowed in 4-Square and 8-Square grid graphs respectively.

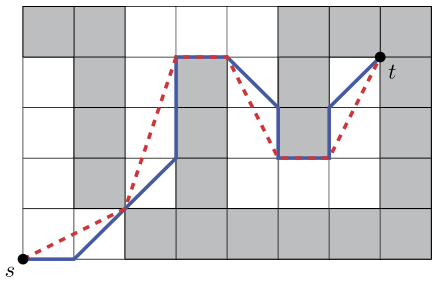

Fig. 3. A true shortest path (red and dashed) and a shortest grid path (blue) in an 8-Square graph that avoids all blocked squares. The paths avoid blocked squares because every part of the path interests with an unblocked square. (For interpretation of the colors in the figure(s), the reader is referred to the web version of this article.)

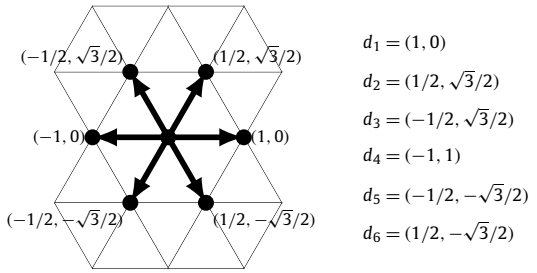

Fig. 4. Movements allowed in 6-Tri grid graphs.

polygons – or through any vertex besides the starting and ending locations – never occurs in a worst-case instance and our results extend even when such movements are not allowed.

This paper bounds how much longer the SGP is than a true shortest path (TSP) – a path that is allowed to move in any direction. In additional to considering square grid graphs, we also consider triangular and hexagonal grid graphs. For triangular grid graphs, traveling along an edge is equivalent to traveling to another vertex in the same triangle. We denote the resulting grid graph as a 6-Tri grid graph as depicted in Fig. 4.

Traveling from a vertex to another vertex of the same hexagon results in the *12-Hex* grid graph described in Fig. 5. At first glance, 12-Hex appears significantly different than 4-Square, 8-Square, and 6-Tri; the set of possible movements depend on the location of the vertex. On closer inspection however, the angles of the movements are identical for every vertex and they only vary in magnitude. Our proofs rely on relaxing the notion of a grid graph by allowing non-integer movements in the directions induced by the grid graph. As such, we need not distinguish between d_i and d'_i when analyzing the 12-Hex grid graph.

Finally, moving along the edges of a hexagon induces the *3-Hex* grid graph described in Fig. 6. The 3-Hex grid graph is fundamentally different than the aforementioned grid graphs as the set of allowed movements are completely different (in angle) for adjacent vertices. As such, the analysis for 3-Hex grid graphs will vary slightly from the other grid graphs.

Prior to analyzing these grid graphs in more detail, we provide a result that simplifies the analysis for all grid paths – including those not mentioned in this paper. We show that when looking for an instance with the worst ratio between the lengths of the SGP and TSP that it suffices to only consider instances where the TSP from the starting point s and the ending point t is a straight line; equivalently when there is line of sight between s and t.

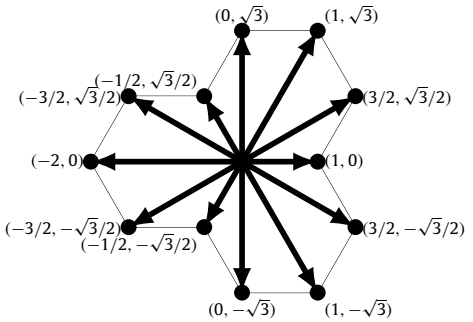

$d_1 = (1, 0)$ $d_7 = (-2, 0)$
$d_2 = (3/2, \sqrt{3}/2)$ $d_8 = (-3/2, -\sqrt{3}/2)$
$d_3 = (1, \sqrt{3})$ $d_9 = (-1/2, -\sqrt{3}/2)$
$d_4 = (0, \sqrt{3})$ $d_{10} = (0, -\sqrt{3})$
$d_5 = (-1/2, \sqrt{3}/2)$ $d_{11} = (1, -\sqrt{3})$
$d_6 = (-3/2, \sqrt{3}/2)$ $d_{12} = (3/2, -\sqrt{3}/2)$

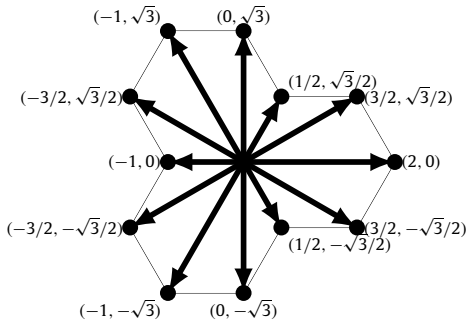

$d'_1 = 2 \cdot d_1$ $d'_7 = d_7/2$
$d'_2 = d_2$ $d'_8 = d_8$
$d'_3 = d_3/2$ $d'_9 = 2 \cdot d_9$
$d'_4 = d_4$ $d'_{10} = d_{10}$
$d'_5 = 2 \cdot d_5$ $d'_{11} = d_{11}/2$
$d'_6 = d_6$ $d'_{12} = d_{12}$

Fig. 5. Movements allowed in 12-Hex grid graphs from the lower left and lower right vertices respectively. While d_i and d'_i may have different magnitudes, they describe movement in the same direction.

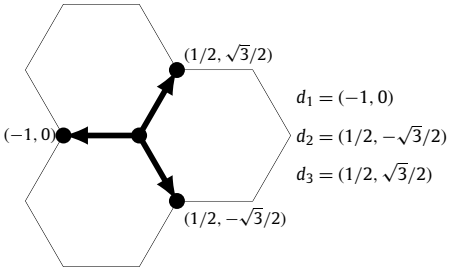

$d_1 = (-1, 0)$
$d_2 = (1/2, -\sqrt{3}/2)$
$d_3 = (1/2, \sqrt{3}/2)$

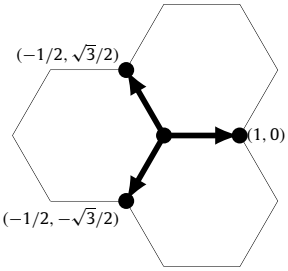

$d_{-1} = -d_1$
$d_{-2} = -d_2$
$d_{-3} = -d_3$

Fig. 6. Movements allowed in 3-Hex grid graphs from the lower left and lower right vertices respectively. Unlike the other grid graphs, the allowed movements are different depending on vertex location.

Theorem 1. *If the (exact or asymptotic) worst-case SGP-to-TSP ratio is α, then for all $\epsilon > 0$ there exists an s and t such that (1) the ratio between the SGP and TSP from s to t is at least $\alpha - \epsilon$ and (2) there are no other vertices are on the TSP from s and t.*

Informally, Theorem 1 states there is worst-case instance where the starting and ending vertices are the only vertices on the TSP. We remark that if the bound is only asymptotically tight then the worst-case ratio is not actually realized and instead there are instances that come arbitrarily close. As such, the use of ϵ in the theorem statement only guarantees that we can select a "worst-case" s and t.

Proof of Theorem 1. For vertices s and t, let $SGP(s, t)$ and $TSP(s, t)$ denote the lengths of a SGP and a TSP between s and t. Let s and t be such that the line segment between s and t contains a minimal number of vertices and where $\frac{SGP(s,t)}{TSP(s,t)} \geq \alpha - \epsilon$. For contradiction, suppose the TSP contains vertex $v \notin \{s, t\}$. Since v is on the TSP between s and t, $TSP(s, t) = TSP(s, v) + TSP(v, t)$. By the triangle inequality, $SGP(s, t) \leq SGP(s, v) + SGP(v, t)$ implying $\frac{SGP(s,t)}{TSP(s,t)} \leq \frac{SGP(s,v)+SGP(v,t)}{TSP(s,v)+TSP(v,t)}$. Therefore, either $\frac{SGP(s,v)}{TSP(s,v)} \geq \frac{SGP(s,t)}{TSP(s,t)} \geq \alpha - \epsilon$ or $\frac{SGP(v,t)}{TSP(v,t)} \geq \frac{SGP(s,t)}{TSP(s,t)} \geq \alpha - \epsilon$. Without loss of generality, suppose $\frac{SGP(s,v)}{TSP(s,v)} \geq \alpha - \epsilon$. The line segment between s and v contains fewer vertices than the line segment between s and t since it excludes t. This, however, contradicts the minimality of the selection of s and t and the statement of theorem holds. □

Informally, Theorem 1 allows individual "segments" of the TSP and SGP to be analyzed independently by splitting the paths whenever they intersect at some vertex besides s and t. For instance, bounding the ratio for the paths in Fig. 7 can be done by analyzing the individual segments of the path – from s to a, from a to b, and from b to t. The ratio between

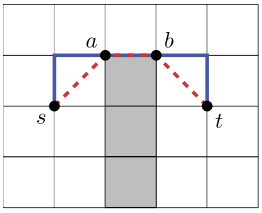

Fig. 7. A true shortest path (red and dashed) and a shortest grid path (blue) in a 4-Square grid graph. The ratio between the SGP and TSP is bounded by the ratio of the segments; $\frac{5}{1+2\sqrt{2}} = \frac{SGP(s,t)}{TSP(s,t)} \leq \max\left\{\frac{SGP(s,a)}{TSP(s,a)}, \frac{SGP(a,b)}{TSP(a,b)}, \frac{SGP(b,t)}{TSP(b,t)}\right\} = \max\left\{\frac{2}{\sqrt{2}}, \frac{1}{1}, \frac{2}{\sqrt{2}}\right\} = \sqrt{2}$.

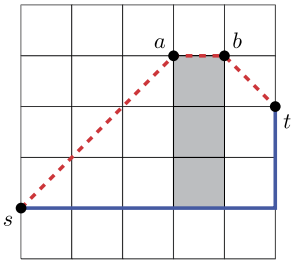

Fig. 8. The shortest grid path does not necessarily stay close to the true shortest grid path. Similar to Fig. 7, we can still bound the ratio between the SGP and TSP based on where the TSP intersects with vertices: $\frac{7}{1+4\sqrt{2}} = \frac{SGP(s,t)}{TSP(s,t)} \leq \max\left\{\frac{SGP(s,a)}{TSP(s,a)}, \frac{SGP(a,b)}{TSP(a,b)}, \frac{SGP(b,t)}{TSP(b,t)}\right\} = \max\left\{\frac{6}{3\sqrt{2}}, \frac{1}{1}, \frac{2}{\sqrt{2}}\right\} = \sqrt{2}$.

the SGP and TSP is then at most the ratio of the SGP and the TSP for the individual segments. As such, when bounding the ratio between the two paths, we may always assume that the paths consist of a single "segment".

Formally however, there is no guarantee that the TSP and SGP intersect anywhere besides s and t even if the TSP passes through another vertex. As seen in Fig. 8, the SGP can deviate greatly from the TSP. Instead, Theorem 1 bounds the ratio in Fig. 8 by constructing three new grid paths for each of the segments in the TSP – a grid path from s to a, a grid path from a to b, and a grid path from b to t. The worst ratio for the paths defined on the pairs $\{s, a\}$, $\{a, b\}$, $\{b, t\}$ then bounds the ratio for the original pair s, t since a grid path from s to a to b to t is a grid path from s to t and therefore at least as long as the shortest grid path from s to t.

3. 8-Square grid graph

In this section, we prove that the worst-case ratio between a shortest grid path (SGP) and a true shortest path (TSP) in an 8-Square grid graph is $\frac{2}{\sqrt{2+\sqrt{2}}}$ and show that this ratio is asymptotically tight (Theorem 7). We consider an ending location t in the cone emanating from the starting location s in the adjacent directions d_1 and d_2 as depicted in Fig. 9.

Without loss of generality, we may always assume this location by rotating the tessellation and/or reflecting the tessellation across the x-axis. Further, our proofs make no use of the values of d_1 or d_2 and the directions $\{d_1, d_2\}$ can be replaced with any pair of adjacent directions, e.g., $\{d_4, d_5\}$ or $\{d_8, d_1\}$. We also only consider s and t where there is line of sight from s to t; by Theorem 1 it suffices to only consider such paths when looking for a worst-case instance. Our proof consists of three parts:

1. If there is a grid path from s to t that only uses directions d_1 and d_2 then it will be a shortest grid path (Theorem 2).
2. There exists a grid path from s to t that only uses directions d_1 and d_2 whenever there is line of sight from s to t (Theorem 3).
3. Given a grid path from s to t that uses only directions d_1 and d_2, the ratio between that grid path and the true shortest path is at most $\frac{2}{\sqrt{2+\sqrt{2}}}$ (Theorem 7).

Before proceeding, we remark that the proofs in this section rely heavily on the lattice structure induced by adjacent directions in an 8-Square grid graph (described in Proposition 4). With the exception of the 3-Hex grid graph, all of our grid graphs form the same lattice structure after applying some linear transformations. In Section 4, we introduce the sufficient properties so that the proofs for 8-Square grid graphs immediately extend to larger family of grid graphs that includes 4-Square, 6-Tri, and 12-Hex, but not 3-Hex. As such, much of the language in this section is written for a general set of directions and for regular polygons that tessellate the plane.

Theorem 2. *Suppose that t is in the cone emanating from s in the adjacent directions d_1 and d_2. If there is an 8-Square grid path from s to t that only uses directions d_1 and d_2, then it is a shortest grid path.*

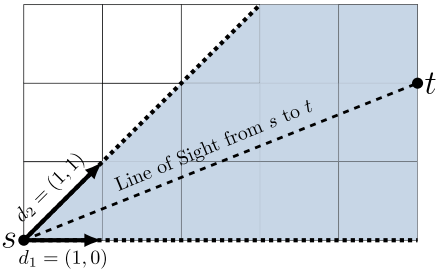

Fig. 9. The blue region shows the cone emanating from s in the directions d_1 and d_2.

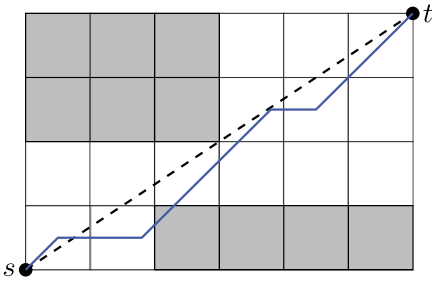

Fig. 10. A relaxed 8-Square grid path from s to t using directions d_1 and d_2.

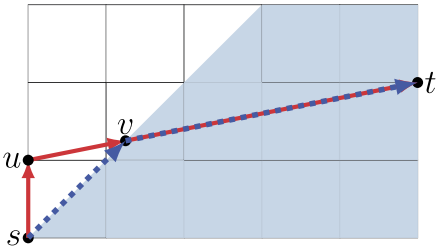

Fig. 11. If a relaxed grid path exits the cone emanating from s, then re-enters at the point u, then we can shorten the path by going directly from s to u using the direction d_1 or d_2. Therefore, the shortest relaxed path must only use d_1 and d_2.

Proof. A grid path is only allowed to use integer multiples of each direction, i.e., we must always move from one corner to point to another corner point in the same polygon in one of the allowed directions. We prove a stronger statement by relaxing the notion of a grid path. Formally we show that if there is an 8-Square grid path from s to t that only uses directions d_1 and d_2, then it is no longer than any path that uses any combination of directions $d_1, ..., d_8$ (not necessarily integer multiples) regardless of whether that path avoids blocked polygons (squares).

We refer to such paths as *relaxed grid paths*; they are still only allowed to move in the same set of directions, but non-integer steps are allowed and the paths are not required to avoid blocked polygons (squares). A relaxed 8-Square grid path is shown in Fig. 10.

Consider a shortest relaxed grid path and suppose it uses direction d_i a total of c_i times. This implies that $t = s + \sum_{i=1}^{8} c_i \cdot d_i$. In particular, since relaxed grid paths are not required to avoid blocked polygons, these directions can be used in any order, e.g., we can start our relaxed grid path by moving in direction d_8, then use all of d_7 and so-on.

For contradiction, let us suppose that there is a shortest relaxed grid path from s to t that is shorter than a grid path that only uses d_1 and d_2, i.e., that there is a shortest relaxed grid path that uses direction d_i where $i \notin \{1, 2\}$. We will show that the relaxed grid path can be made shorter, a contradiction:

Since the path uses d_i where $i \notin \{1, 2\}$, we can assume it uses the direction d_i first since the relaxed grid path is not required to avoid blocked polygons. Since d_1 and d_2 are adjacent directions, the relaxed grid path reaches a point u that is outside the cone emanating from s in the directions d_1 and d_2. Since t is inside this cone, there must be a point on the relaxed grid path, v, that appears after u and appears on the boundary of the cone. However, this contradicts that we have a shortest relaxed grid path; since v is on the boundary of the cone, the shortest s to v relaxed grid path uses only direction d_1 or d_2 and therefore we can shorten our path to avoid the point u by going directly from s to v as depicted in Fig. 11.

This implies that a shortest relaxed grid path uses only d_1 and d_2. Next, observe that if two different relaxed grid paths use only d_1 and d_2 then they have the same length since d_1 and d_2 are linearly independent. Finally, every grid path is also

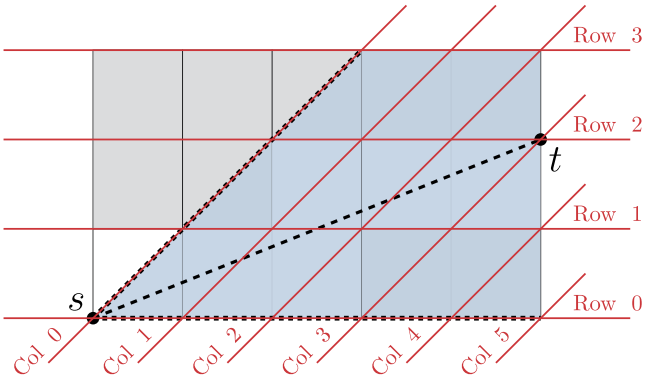

Fig. 12. Parallelogram grid induced by d_1 and d_2 with "rows" and "columns" in the respective directions.

a relaxed grid path. Thus, if there is a grid path that uses only d_1 and d_2, then it is a shortest relaxed grid path and no longer than any other grid path. □

Theorem 3. *Suppose that t is in the cone emanating from s in the adjacent directions d_1 and d_2 as shown in Fig. 9. If there is line of sight from s to t, then there is a grid path from s to t that uses only d_1 and d_2.*

Theorems 2 and 3 imply that the shortest grid path from s to t uses only directions d_1 and d_2 if there is line of sight between s and t thereby allowing easy computation of the length of the shortest grid path. Note that if t is on the boundary of the cone, then $t = s + c_i \cdot d_i$ for either $i = 1$ or $i = 2$ and the TSP and SGP are identical yielding a SGP-TSP ratio of one. Thus, our analysis focuses on t in the interior of the cone. Before proceeding, we introduce the lattice structure induced by the adjacent directions d_1 and d_2.

Proposition 4 *(Parallelogram Grid Graph for 8-Square). For any vertex t in the cone emanating from s in the adjacent directions d_1 and d_2, t can be reached from s using only the directions d_1 and d_2 when there are no blocked polygons.*

Proposition 4 is readily shown by induction and the proof is deferred to the appendix. In particular, this means that d_1 and d_2 induce a *parallelogram grid* in the cone emanating from s where the lattice points of the grid are precisely the vertices of the original grid graph as depicted in Fig. 12.

We now prove Theorem 3 by providing an algorithm that finds such a path from s to t using d_1 and d_2. Let $a \in \mathbb{R}^2$ and $b \in \mathbb{R}$ be such that the line of sight from s to t is written as $\{x : a^\intercal x = b\}$ where $a^\intercal d_1 \leq 0$ (direction d_1 moves below the line) and $a^\intercal d_2 \geq 0$. Then Algorithm 1 finds an 8-Square grid path from s to t whenever there is line of sight. Algorithm 1 works by staying above the line of sight, but as close as possible to ensure that it does not traverse any blocked polygons as shown in Fig. 13.

Algorithm 1 Finding a Shortest Grid Path by Staying Above the Line of Sight.

```
1: procedure FIND GRID PATH
2:     i ← 0
3:     v_i ← s
4:     while v_i ≠ t do
5:         if a^⊺(v_i + d_1) ≥ b (equivalently, v_i + d_1 on or above the line of sight) then
6:             v_{i+1} ← v_i + d_1
7:         else
8:             v_{i+1} ← v_i + d_2
9:         i ← i + 1
```

Lemma 5. *Algorithm 1 terminates when t is in the interior of the cone emanating from s in the directions d_1 and d_2.*

Proof. Suppose t is in row k. Since t is in the interior of the cone, the line $a^\intercal x = b$ is not parallel to d_1 or row k. Thus, t is the unique point on $a^\intercal x = b$ and in row k. By design of Algorithm 1, $a^\intercal v_m \geq b$ for each iteration. Therefore, if the algorithm fails to terminate, there must be an m such that v_m is in row $k+1$. Select m minimally. By minimality, $v_m = v_{m-1} + d_2$ where $v_{m-1} \neq t$ is in row k. Since v_m is added to the path, $a^\intercal(v_{m-1} + d_1) < b$. However, this implies that $a^\intercal x = b$ intersects row k strictly between adjacent vertices v_{m-1} and $v_{m-1} + d_1$. This implies that t is not a vertex in the graph, a contradiction. □

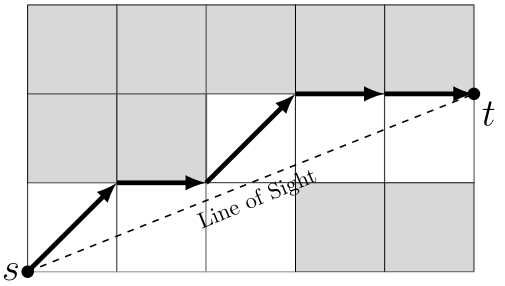

Fig. 13. Grid path found by Algorithm 1 by staying close to the line of sight. Algorithm 1 behaves similarly to Bresenham's line algorithm; the traversed polygons can be used to define a pixel representation of $\overline{st}$.

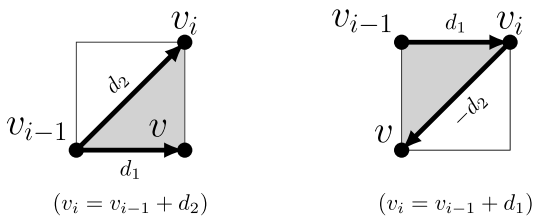

Fig. 14. Selection of v for Lemma 6. The points v, v_{i-1}, and v_i form a triangle contained inside a unique polygon.

Lemma 6. *Suppose t is in the interior of the cone emanating from s in the directions d_1 and d_2 and there is line of sight between s and t. For each v_{i-1} and v_i added in Algorithm 1, the line segment $\overline{v_{i-1}v_i}$ also does not intersect with any blocked polygons*

Proof. Similar to Theorem 1, without loss of generality, we may assume that the line of sight only intersects with the vertices s and t. If not, it intersects with vertex $v \notin \{s, t\}$ and the analysis can be conducted separately on the segments $\overline{sv}$ and $\overline{vt}$. We break the proof into two parts depending on whether $v_i = v_{i-1} + d_2$ or $v_i = v_{i-1} + d_1$. Both parts involve finding a polygon P containing both v_i and v_{i-1} where the line of sight from s to t enters the interior of P implying that P is not blocked thereby proving the statement of the theorem.

Case 1: $v_i = v_{i-1} + d_2$. Suppose first that $v_i = v_{i-1} + d_2$ and let $v = v_{i-1} + d_1$. Since d_1 and d_2 are adjacent, there is a unique polygon P with corners v_i, v_{i-1} and v as depicted in Fig. 14. By selection of v_{i-1} and v, $a^\intercal v_{i-1} \geq b$ and $a^\intercal v < b$ implying that the line of sight intersects with the line segment $\overline{v_{i-1}, v}$ at some location other than v since $a^\intercal < b$. By definition, $\overline{v_{i-1}, v}$ is parallel to d_1 which is not parallel to the line of sight. Since line of sight between s and t is between the directions d_1 and d_2 and doesn't pass through v, the line of sight also enters the interior of the triangle defined by v_i, v_{i-1} and v. Since the polygons are convex, this triangle is necessarily in P and therefore P is not blocked completing the first part of the lemma.

Case 2: $v_i = v_{i-1} + d_1$. Now suppose that $v_i = v_{i-1} + d_1$. Let $v = v_i - d_2$ and thus there is a unique polygon P containing v_{i-1}, v_i, and v as depicted in Fig. 14. Next, we show that $a^\intercal v < b$. Suppose v_i is in row k and let v_j be last vertex added by Algorithm 1 that is in row $k-1$ as depicted in Fig. 15. Equivalently, j is the largest index such that $v = v_j + c \cdot d_1$ for some $c \geq 1$. By the maximality of j, $v_{j+1} = v_j + d_2$ and therefore $a^\intercal(v_j + d_1) < b$. This implies that $a^\intercal v = a^\intercal(v_j + c \cdot d_1) = a^\intercal(v_j + d_1) + a^\intercal(c-1)d_1 < b + 0 = b$. Thus, the line of sight must intersect with the line segment $\overline{v_i, v}$ at some location over than v since $a^\intercal v_i \geq b$. By symmetry, s is in the cone emanating from t in the directions $-d_1$ and $-d_2$. Following identically to the previous case, the line of sight $\overline{st}$ must enter the triangle defined by v_i, v_{i-1}, and v. This triangle is necessarily in P and therefore P is not blocked completing the lemma. □

Theorem 3 now follows directly from Lemmas 5 and 6; Algorithm 1 finds a grid path from s to t that uses only directions d_1 and d_2. This path avoids all blocked polygons since each line segment added intersects with a polygon that is traversed by the line of sight from s to t. Finally, we determine the worst-case ratio between the SGP and the TSP.

Theorem 7. *For the 8-Square graph where the angle between d_1 and d_2 is $\theta = \pi/4$, the ratio between the lengths of a SGP and a TSP is at most $\sqrt{\frac{2}{1+\cos\theta}} = \frac{2}{\sqrt{2+\sqrt{2}}} \approx 1.0824$. This ratio is asymptotically tight.*

Proof. By Theorems 1, 2, and 3, it suffices to show the result when there are no blocked polygons and when there is line of sight. Without loss of generality, suppose t is in the cone emanating from s in the direction d_1 and d_2 and $t = s + c_1 \cdot d_1 + c_2 \cdot d_2$ for some integer $c_i > 0$. By Theorems 2 and 3, the shortest path uses only directions d_1 and d_2 and therefore has length

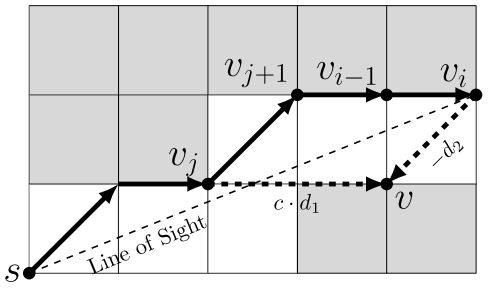

Fig. 15. Selection of v and v_j when $v_i = v_{i-1} + d_1$ in Lemma 6.

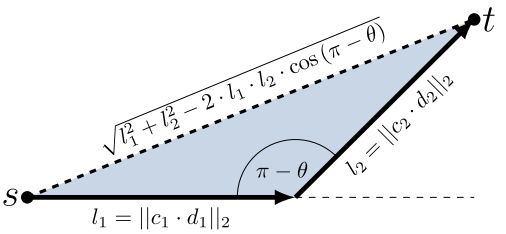

Fig. 16. Ratio between the true shortest path and the shortest grid path.

$l_1 + l_2$ where $l_i = ||c_i \cdot d_i||_2$. By the law of cosines, the length of the true shortest path is $\sqrt{l_1^2 + l_2^2 - 2 \cdot l_1 \cdot l_2 \cdot \cos(\pi - \theta)}$ as depicted in Fig. 16.

Thus, the ratio between the true shortest path and the shortest grid path is

$$\frac{l_1 + l_2}{\sqrt{l_1^2 + l_2^2 - 2 \cdot l_1 \cdot l_2 \cdot \cos(\pi - \theta)}} = \frac{l_1 + l_2}{\sqrt{l_1^2 + l_2^2 + 2 \cdot l_1 \cdot l_2 \cdot \cos(\theta)}}$$

To bound this ratio, it suffices to solve:

$$\max_{(l_1, l_2) \in \mathbb{R}^2_{\geq 0}} \frac{l_1 + l_2}{\sqrt{l_1^2 + l_2^2 + 2 \cdot l_1 \cdot l_2 \cdot \cos(\theta)}} \tag{1}$$

The maximizer of (1) also solves

$$\min_{(l_1, l_2) \in \mathbb{R}^2_{\geq 0}} \frac{l_1^2 + l_2^2 + 2 \cdot l_1 \cdot l_2 \cdot \cos(\theta)}{(l_1 + l_2)^2} = \inf_{w \geq 0} \min_{\substack{(l_1, l_2) \in \mathbb{R}^2_{\geq 0}: \\ l_1 + l_2 = \sqrt{w}}} \frac{l_1^2 + l_2^2 + 2 \cdot l_1 \cdot l_2 \cdot \cos(\theta)}{w}, \tag{2}$$

since (2) is attained by taking the reciprocal and the square (two monotonic transformations) of (1). The domain $\{(l_1, l_2) \in \mathbb{R}^2_{\geq 0} : l_1 + l_2 = \sqrt{w}\}$ is symmetric and convex and the function $l_1^2 + l_2^2 + 2 \cdot l_1 \cdot l_2 \cdot \cos(\theta)$ is symmetric and strictly convex for $\theta \in (0, \pi/2)$. Therefore, all optimal solutions to (2) are symmetric ($l_1 = l_2$) and (1) simplifies to

$$\max_{l_1 \in \mathbb{R}_{\geq 0}} \frac{2l_1}{\sqrt{2l_1^2 + 2 \cdot l_1^2 \cdot \cos(\theta)}} = \sqrt{\frac{2}{1 + \cos\theta}} \tag{3}$$

as in the statement of the theorem.

Finally we remark that this bound is only asymptotically tight. Since the function in (2) is strictly convex, it is only possible to build a worst-case example when $l_1 = l_2$ implying that t is on the bisector of d_1 and d_2. However, the slope of the bisector is irrational and therefore no integer points (besides s) appear on the bisector and thus the worst-case ratio cannot be attained. The ratio is asymptotically tight however since a line with an irrational slope comes arbitrarily close to infinitely many integer points [37]. □

4. Parallelogram grid graphs

In this section, we identify the necessary properties to extend the results of Section 3 to the 6-Tri, 4-Square, and 12-Hex grid graphs. More generally, the proofs and theorems of Section 3 extend to any *parallelogram grid graph* – even variants where the plane is tessellated by non-regular or even varying convex shapes.

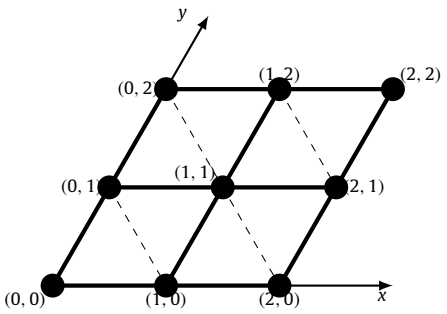

Fig. 17. Labeling of $\mathbb{R}^2$ in the basis induced by $d_1 = (1, 0)$ and $d_2 = (3/2, \sqrt{3}/2)$.

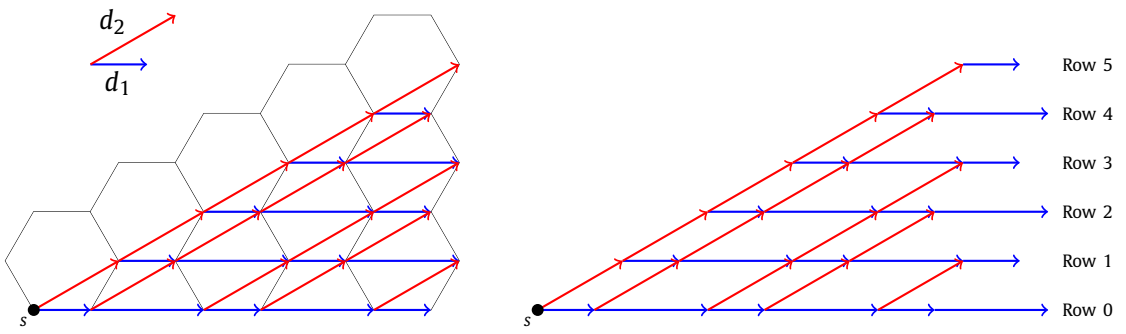

Fig. 18. Parallelogram Grid Structure of 12-Hex Grid Graphs.

Definition 1 *(Parallelogram Grid Graph).* A grid graph is a parallelogram grid graph if it satisfies the following properties when there are no blocked polygons.

[P1] The angle (not necessarily magnitude) of allowed movements is independent of the vertex location.
[P2] For each direction, backwards movement is allowed, i.e., if d_i is an allowed movement, then $-d_i$ (subject to rescaling) is also allowed.
[P3] For vertex v and adjacent directions d_1 and d_2, there exists a polygon containing v, $v + d_1$, and $v + d_2$.
[P4] For adjacent directions d_1 and d_2, starting vertex s, and every vertex v in the cone emanating from s in the directions d_1 and d_2, v can be reached from s using only directions d_1 and d_2.

For 6-Tri, 4-Square, and 8-Square, property [P1] holds immediately. To see that the property holds for 12-Hex, observe that the allowed movements at each vertex only vary in magnitude and not angle, e.g., movement to the right can correspond to moving by (1,0) or (2,0) depending on the vertex. Similarly, properties [P2] and [P3] are easily verified by observation for each grid graph. Finally, property [P4] is shown for all grid graphs in the appendix.

We remark that this formulation essentially reduces hexagonal and triangular grid graphs to a square grid graph by redefining the set of basis vectors that we use to label $\mathbb{R}^2$. In the case of 6-Tri graph, every vertex is an integer point in the basis induced by $d_1 = (1, 0)$ and $d_2 = (3/2, \sqrt{3}/2)$ as depicted in Fig. 17.

Similarly, every vertex is a 12-Hex grid graph is also a lattice point in the basis induced by two adjacent directions as shown in Fig. 18. We formalize these bases in the appendix while proving [P4] for each of the graphs. Further, [P1]–[P3] ensure that movement in the basis induced by d_1 and d_2 looks identical to movement in a 4-Square grid graph with rows and columns. As such, the framework we introduce in Definition 1 allows analysis conducted on square grid graphs to be extended to triangular, hexagonal, and even irregular grid graphs, e.g., stretched rectangles/parallelograms as is the case in 12-Hex (Fig. 18). Using this framework, our results in the previous section readily extend to all parallelogram grid graphs.

Theorem 8. *Consider any parallelogram grid graph. Suppose that t is in the cone emanating from s in the adjacent directions d_1 and d_2. If there is an $s - t$ grid path that only uses directions d_1 and d_2, then it is a shortest grid path.*

This proof follows identically to Theorem 2; the proof only makes use of properties [P1] and [P4] to guarantee that you can shortcut any path that leaves the cone and re-enters at point v by traveling directly from s to v in the direction d_1 or d_2. We remark that the magnitude of the direction was never used in the proof – the proof was shown for a relaxed grid path where only the direction of movement matters.

Table 2
Worst-Case Ratios for Analyzed Parallelogram Grid Graphs.

Grid Graph	Angle Between Directions	Worst-Case Ratio Between SGP and TSP	
4-Square	$\pi/2$	$\sqrt{\frac{2}{1+\cos(\pi/2)}} = \sqrt{2} \approx 1.4142$	(tight)
6-Tri	$\pi/3$	$\sqrt{\frac{2}{1+\cos(\pi/3)}} = \frac{2}{\sqrt{3}} \approx 1.1547$	(tight)
8-Square	$\pi/4$	$\sqrt{\frac{2}{1+\cos(\pi/4)}} = \frac{2}{\sqrt{2+\sqrt{2}}} \approx 1.0824$	(asymptotically tight)
12-Hex	$\pi/6$	$\sqrt{\frac{2}{1+\cos(\pi/6)}} = \sqrt{6}-\sqrt{2} \approx 1.0353$	(asymptotically tight)

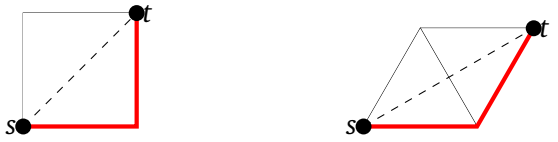

Fig. 19. Worst case SGP-to-TSP ratio for 4-Square and 6-Tri respectively.

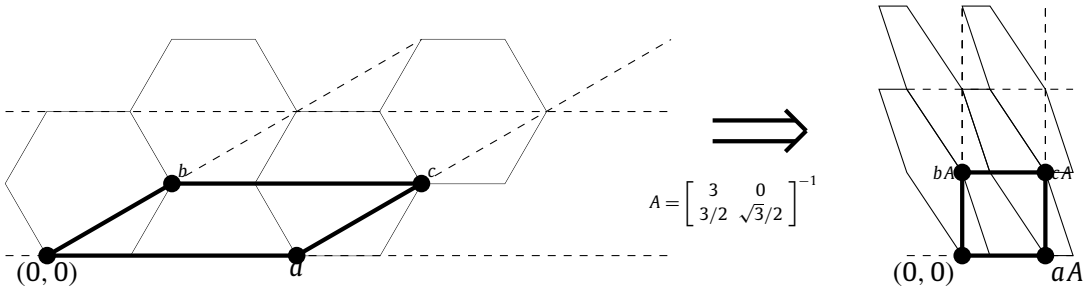

Fig. 20. Transforming 12-Hex so that all vertices are rational and all integer points are vertices.

Theorem 9. *Consider any parallelogram grid graph. Suppose that t is in the cone emanating from s in the adjacent directions d_1 and d_2. If there is line of sight from s to t, then there is a grid path from s to t that uses only d_1 and d_2.*

Theorem 9 follows identically to Theorem 3 by using Algorithm 1 to find the path. Lemma 5 guarantees that Algorithm 1 terminates by making use of the parallelogram grid structure induced by property [P4] and therefore extends to all parallelogram grid graphs. Moreover, each line segment added in Algorithm 1 intersects with no blocked polygons as in Lemma 6. This lemma makes use of Property [P3] in order to find an unblocked polygon that contains the added line segment – in one case, it also uses Property [P2] by moving backwards in a direction to find the unblocked polygon. As such, Lemma 6 extends to all parallelogram grid graphs and Theorem 9 holds.

Theorem 10. *Consider any parallelogram grid graph. Suppose that t is in the cone emanating from s in adjacent directions d_1 and d_2 and let θ be the angle between d_1 and d_2. The ratio between the lengths of the SGP and TSP is at most $\sqrt{\frac{2}{1+\cos\theta}}$. Moreover, this ratio is tight if there is a vertex along the bisector of d_1 and d_2.*

Theorem 10 follows identically to Theorem 7. In particular, for the parallelogram grid graphs referenced in this paper, the worst-case ratios are given in Table 2. Unsurprisingly, the worst-case ratio decreases as the angle between adjacent angles decreases – equivalently, as more directions of movement are allowed in the grid graph.

The worst-case ratios for 4-Square and 6-Tri are shown in Fig. 19. Demonstrating that the bound for the 12-Hex grid graph is asymptotically tight follows almost identically to the 8-Square after applying a transformation. We first map the set of hexagons into a new basis via the linear transformation $A = \begin{bmatrix} 3 & 0 \\ 3/2 & \sqrt{3}/2 \end{bmatrix}^{-1}$ as demonstrated in Fig. 20. After this transformation, each vertex of a hexagon maps to a rational point in the new basis and each integer point coordinate in the new space maps to a vertex of the transformed hexagons. Specifically, when proving [P4] for 12-Hex in the appendix, we show that the lower left vertices of hexagons map form the set of integer points in the new basis and that every lower right vertex located $(1,0)A = (1/3, 0)$ from a lower left vertex.

In the original space, a bisector of $d_1 = (1,0)$ and $d_2 = (3/2, \sqrt{3}/2)$ is $(2-\sqrt{3}, 1)$. After the linear transformation, the bisector corresponds to the vector $(2-\sqrt{3}, 1)A = (2/3 - 2/\sqrt{3}, 2/\sqrt{3})$, which has an irrational slope. The argument now follows identically to 8-Square by working in the transformed space. With $s = (0,0)$, no other rational points appear on the bisector and, since all hexagon vertices are rational in the transformed space, no other vertices appear on the bisector. Thus,

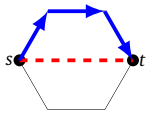

Fig. 21. The SGP in the 3-Hex grid graph may require movement in three directions.

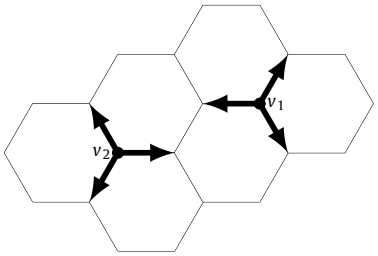

Fig. 22. $label(v_1) = +1$, $label(v_2) = -1$.

Table 3
Directions available based on the label of v.

$label(v) = +1$	$label(v) = -1$
$d_{+1} = (-1, 0)$	$d_{-1} = (1, 0)$
$d_{+2} = \left(\frac{1}{2}, \frac{\sqrt{3}}{2}\right)$	$d_{-2} = \left(-\frac{1}{2}, -\frac{\sqrt{3}}{2}\right)$
$d_{+3} = \left(\frac{1}{2}, -\frac{\sqrt{3}}{2}\right)$	$d_{-3} = \left(-\frac{1}{2}, \frac{\sqrt{3}}{2}\right)$

the worst-case ratio cannot be achieved. However, the bisector comes arbitrarily close to infinitely many integer points in the transformed space. Since all integer points correspond to vertices of hexagons, the ratio can be made arbitrarily close to the ratio in Table 2.

5. 3-Hex grid graphs

Unlike the other 2D grid graphs, the 3-Hex grid graph does not satisfy the parallelogram grid properties; it only satisfies [P3]. As a result, the parallelogram grid graph may require three different directions to be used in the shortest grid path as demonstrated in Fig. 21.

We begin by characterizing the set of directions used in a SGP. Property [P1] does not hold for 3-Hex graphs and the path is not allowed to move in the same set of directions at each vertex. To address this inconsistency, we label each vertex with ± 1 to indicate the set of allowed movements. This labeling is shown in Fig. 22 and corresponds to lower left vertices (-1) and lower right vertices $(+1)$. If $label(v) = +1$, then a path at v can move in directions d_{+i} for $i = 1, 2, 3$ where each direction is defined in Table 3. Similarly, if $label(v) = -1$, then a path at v can move in directions d_{-i} for $i = 1, 2, 3$.

As shown in Fig. 21, three directions may be required to get from s to t in a 3-Hex grid graph. However, a SGP will never use four directions when there are no blocked hexagons. Specifically, if direction d_i is used, then direction d_{-i} is not used for $i \in \pm\{1, 2, 3\}$.

Theorem 11. *If a shortest grid path from s to t uses direction d_i, then it does not use d_{-i} when there are no blocked hexagons.*

Proof. We consider a path using both directions d_{+1} and d_{-1}. We then show that we can re-arrange the path so that d_{+1} and d_{-1} are the first two directions remove. However, this implies that after two steps, the path returns to the starting node s and therefore the path can be shortened by removing these two directions.

A shortest grid path from s to t is described by a sequence of directions $(d_{j_1}, d_{j_2}, ..., d_{j_n})$, i.e., $t = s + \sum_{i=1}^{n} d_{j_i}$ where $v'_k = s + \sum_{i=1}^{k} d_{j_i}$ is the kth vertex visited on the path. If v and v' are adjacent, then $label(v) = -label(v')$ and therefore j_i and j_{i+1} have opposite signs for all i. By reflecting s, t, and the tessellation of hexagons across a vertical axis, we may assume that $label(s) = +1$, $j_i < 0$ for i even, and $j_i > 0$ for i odd. Let σ be a permutation of $J = \{j_1, ..., j_n\}$ such that $\sigma_i < 0$ for i even and $\sigma_i > 0$ for i odd – equivalently, j_i and σ_i have the same sign.

First observe that σ still describes a valid 3-Hex grid path from s to t; by selection, $t = s + \sum_{i=1}^{n} d_{j_i} = s + \sum_{i=1}^{n} d_{\sigma_i}$ since σ is a permutation of J. It remains to show that σ corresponds to a valid path. Let $v_k = s + \sum_{i=1}^{k} d_{\sigma_i}$. We will show by induction that (1) v_k is a vertex of a hexagon, (2) $label(v_k) = -1$ for k odd and $+1$ for k even, and (3) v_k is reached from v_{k-1} using an allowed direction at v_{k-1}. By selection of σ, v_1 is a vertex of a hexagon since $\sigma_i > 0$ and $label(s) = +1$. By induction, for k even, v_{k-1} is a vertex and $label(v_{k-1}) = -1$. Further, $\sigma_{k-1} < 0$ since k is even. Since $label(v_{k-1}) = -1$, moving in direction σ_{k-1} describes a valid movement to an adjacent vertex. Therefore $v_k = v_{k-1} + d_{\sigma_{k-1}}$

is a vertex. Moreover, $label(v_k) = +1$ since its it is adjacent to a vertex with a label of -1 thereby completing the claim for k even. The proof for k odd follows identically. Therefore, σ corresponds to a valid path from s to t.

Finally, we show that if direction d_i is used in a shortest grid path, then d_{-i} is not. For contradiction, suppose there is a shortest grid path from s to t described by the sequence $J = (j_1, .., j_n)$ with an odd k and even l such that $j_k = -j_l$, i.e. the direction d_i and d_{-i} is used for $i = j_k$. Select a permutation, σ, of J such that the sign of j_i is the same as σ_i for all i and such that $\sigma_1 = j_k$ and $\sigma_2 = j_l$. By the previous claim, σ describes a valid path from s to t. Moreover it is also a shortest grid since all directions have the same length. Let $v_k = s + \sum_{i=1}^{k} d_{\sigma_i}$. Thus, $v_2 = s + d_{j_k} + d_{j_l} = s + d_{j_k} + d_{-j_k} = s + d_{j_k} + -d_{j_k} = s$. This implies that $(\sigma_3, ..., \sigma_n)$ describes a valid path from s to t contradicting that σ is a shortest grid path. Therefore, if direction d_i is used in a shortest grid path, then d_{-i} is not. □

Theorem 11 is similar to Theorem 2 in that it provides a characterization of the set of directions used to optimally travel from s to t. Using this connection, we prove that the worst-case ratio between the lengths of the SGP and the TSP is $\frac{3}{2}$ and converges to $\frac{4}{3}$ as the length of the SGP tends to infinity.

Theorem 12. *For 3-Hex grid graphs, the ratio between lengths of a SGP and a TSP is at most $\frac{3}{2}$ when there are no blocked hexagons. Furthermore, the worst-case ratio converges to $\frac{4}{3}$ as the length of the SGP tends to infinity.*

Proof. Let $J = \{j_1, ..., j_n\}$ describe a shortest grid path from s to t as in the proof of Theorem 11. We consider only paths with length at least two since otherwise s is adjacent to t and the SGP and TSP are the same path. As in the proof of Theorem 11, we may assume $label(s) = +1$ and therefore $j_1 > 0$. Moreover, after rotating s, t, and the tessellation of hexagons around the point s by a multiple of $2\pi/3 = 120°$, we may assume $d_{j_1} = d_{+1} = (-1, 0)$. Further, by reflecting across a horizontal axis, we may assume $d_{j_2} = d_{-2} = \left(-\frac{1}{2}, -\frac{\sqrt{3}}{2}\right)$. By Theorem 11, J contains at most one other distinct element and it is either d_{+3} or $d_{-3} = -d_{+3} = \left(-\frac{1}{2}, \frac{\sqrt{3}}{2}\right)$.

Case 1: d_{+1}, d_{-2}, and d_{+3} appear in J. Let k be the length of the SGP – equivalently the number of elements in the sequence J – and let c_i denote the number of times d_i appears in J implying $c_{+1} + c_{-2} + c_{+3} = k$. As in Theorem 11, j_i and j_{i+1} have opposite signs and therefore approximately half of the elements of J are $\{-2\}$. Specifically, $j_1 > 0$ since $label(s) = +1$ and $c_{+1} + c_{+3} = c_{-2} + r$ where $r = k \mod 2$. Combining both equalities, $c_{-2} = \frac{k-r}{2}$ and $c_{+3} = k - c_{+1} - c_{-2} = k - c_{+1} - \frac{k-r}{2}$. This implies

$$\begin{aligned}
t - s &= c_{+1} \cdot d_{+1} + c_{-2} \cdot d_{-2} + c_{+3} \cdot d_{+3} \\
&= c_{+1} \cdot (-1, 0) + c_{-2} \cdot (-1/2, -\sqrt{3}/2) + c_{+3} \cdot (1/2, -\sqrt{3}/2) \\
&= \left(-c_{+1} - \frac{c_{-2}}{2} + \frac{c_{+3}}{2}, -\frac{(c_{+3} + c_{-2})\sqrt{3}}{2} \right) \\
&= \left(-c_{+1} - \frac{k-r}{4} + \frac{k - c_{+1} - \frac{k-r}{2}}{2}, -\frac{(k - c_1)\sqrt{3}}{2} \right) \\
&= \frac{1}{2} \left(r - 3c_{+1}, (c_{+1} - k)\sqrt{3} \right)
\end{aligned}$$

and therefore the length of the TSP is $\frac{\sqrt{(r-3c_{+1})^2 + 3(c_{+1}-k)^2}}{2}$. The length of the shortest grid paths is k since J contains k elements. Thus, the ratio between the two paths is

$$\frac{k}{||t - s||_2} = \frac{2k}{\sqrt{(r - 3c_{+1})^2 + 3(c_{+1} - k)^2}} \leq \frac{4k}{3k - r} \tag{4}$$

where (4) follows by minimizing $(r - 3c_{+1})^2 + 3(c_{+1} - k)^2$ with respect to c_{+1} with $c^*_{+1} = \frac{k+r}{4}$. For $r = 0$ (k even), (4) reduces to $\frac{4}{3}$. For $r = 1$ (k odd), (4) reduces to $f(k) = \frac{4k}{3k-1} \to \frac{4}{3}$ as $k \to \infty$. Moreover, $f(k)$ is maximal when $k = 3$ yielding $f(3) = \frac{3}{2}$. The ratio $\frac{3}{2}$ is demonstrated to be tight in Fig. 23. This completes the proof of the theorem when J consists only of the directions d_{+1}, d_{-2}, and d_{+3}.

Case 2: d_{+1}, d_{-2}, and d_{-3} appear in J. This case follows identically to case 1. Denote k, c_i, and r as before implying $c_{+1} = \frac{k+r}{2}$ (at least half the steps use c_{+1} since $j_1 > 0$) and $c_{-3} = k - c_{+1} - c_{-2} = k - \frac{k+r}{2} - c_{-2}$. Therefore,

$$\begin{aligned}
t - s &= c_{+1} \cdot d_{+1} + c_{-2} \cdot d_{-2} + c_{-3} \cdot d_{-3} \\
&= c_{+1} \cdot (-1, 0) + c_{-2} \cdot (-1/2, -\sqrt{3}/2) + c_{-3} \cdot (-1/2, \sqrt{3}/2)
\end{aligned}$$

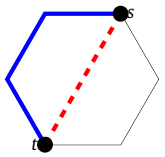

Fig. 23. Worst-case SGP-to-TSP ratio for 3-Hex grid graphs.

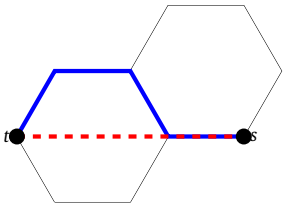

Fig. 24. Repeatable path demonstrating 4/3 ratio for long paths.

$$= \left(-\frac{3k}{4} - \frac{r}{4}, \frac{(k-r)\sqrt{3}}{4} - c_{-2}\sqrt{3} \right)$$

and the ratio between the lengths of the shortest grid path and the true shortest path is

$$\frac{k}{||t-s||_2^2} = \frac{4k}{\sqrt{(3k+r)^2 + 3(k-r-4c_{-2})^2}} \tag{5}$$

$$\leq \frac{4k}{3k+r} \leq \frac{4}{3} \tag{6}$$

The inequalities in ((5)–(6)) hold since $3(k-r-4c_{-2})^2 \geq 0$ thereby completing the proof of the theorem. We also remark that, in the limit that the 4/3 ratio is tight and can be seen by extending the line in Fig. 24. □

Finally, we show that the set of blocked hexagons has no impact on the shortest grid path if there is line of sight between s and t. We first establish that if a grid path from s to t uses the same set of directions as an SGP from s to t, then it also an SGP; this result is similar to the linear independence that we used for the parallelogram grid graphs. We then convert a 12-Hex SGP from s to t from Algorithm 1 into a 3-Hex grid path that (1) respects avoids blocked hexagons and (2) uses the same set of directions as an SGP from s to t. Together, these things imply that the blocked polygons have no impact on the shortest grid path and the worst-case ratios from Theorem 12 extend even when there are blocked hexagons.

Lemma 13. *Suppose there is an SGP from s to t that uses only the directions $d_{\pm i}$ for $i = 1, 2, 3$ as given in the proof of Theorem 12. Then every path from s to t that uses the same set of directions is also an SGP.*

Proof. Through rotational symmetry, we may assume there is a shortest path from s to t using only the directions d_{+1}, d_{-2}, and d_{-3} – unlike Theorem 12, we make no assumption about the label of s and we can assume the third direction is d_{-3}.

Consider any path from s to t that use only directions d_{+1}, d_{-2}, and d_{-3} and let c_i be the number of times each coefficient is used. Equivalently,

$$t - s = c_{+1} \cdot d_{+1} + c_{-2} \cdot d_{-2} + c_{-3} \cdot d_{-3}.$$

Similar to Theorem 12, $c_{+1} = c_{-2} + c_{-3} + q$ where $q \in \{-1, 0, 1\}$. We now focus on the first coordinate of $t - s$. Specifically, by construction of 3-Hex, $2(t_1 - s_1)$ is integer. By definition of $d_{\pm i}$,

$$2(t_1 - s_1) = -2 \cdot c_{+1} - (c_{-2} + c_{-3}) = -3 \cdot c_{+1} + q \equiv q \mod 3.$$

Thus $q \in \{-1, 0, 1\}$ is uniquely determined by s and t. This implies c_{+1} is uniquely determined by s and t since $2(t_1 - s_1) = 3 \cdot c_{+1} + q$. Further, $c_{-2} + c_{-3} = c_{+1} - q$ is also determined uniquely by s and t. Finally, the length of the path, $c_{+1} + (c_{-2} + c_{-3})$ is a unique constant determined only by s and t. Therefore all grid paths that use the same set of directions as a SGP are also SGPs. □

Finally, we show that blocked hexagons have no impact on the length of an SGP when there is line of sight between s and t. We accomplish this by converting the 12-Hex grid path from Algorithm 1 into a 3-Hex grid path.

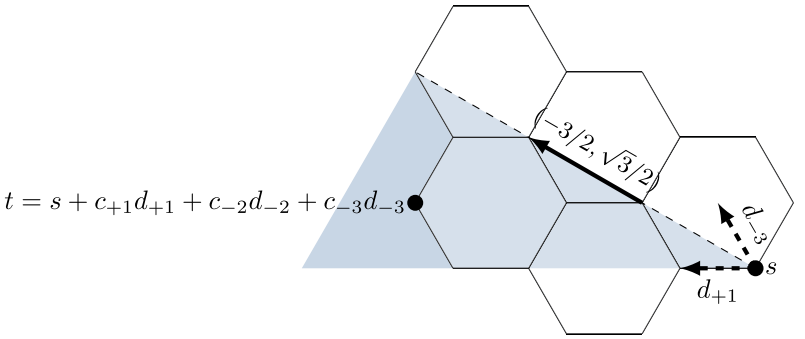

Fig. 25. Vertex t is in the cone emanating from s in the directions $d_{+1} = (-1, 0)$ and $(-3/2, \sqrt{3}/2)$.

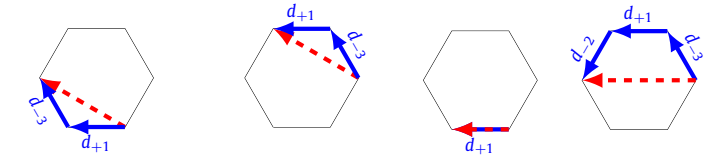

vertex label: -1 direction $(-3/2, \sqrt{3}/2)$ | vertex label: $+1$ direction $(-3/2, \sqrt{3}/2)$ | vertex label: -1 direction $(-1, 0)$ | vertex label: $+1$ direction $(-2, 0)$

Fig. 26. Converting a 12-Hex grid path to a 3-Hex grid path (case 1).

Theorem 14. *If there is line of sight from s to t, then blocked hexagons have no effect on the length of an SGP from s to t in a 3-Hex Grid Graph.*

Proof. Without loss of generality, suppose that a SGP from s to t only uses directions d_{+1}, d_{-2}, and d_{-3} when blocked hexagons are ignored. Let c_i denote the number of times d_i is used. By reflecting across a horizontal axis, we may also assume that $c_{-3} \geq c_{-2}$; this reflections swaps d_{-2} and d_{-3} in the grid path and there is still a shortest grid path using only directions d_{+1}, d_{-2}, and d_{-3}. Moreover, $c_{+1} = c_{-2} + c_{-3} + q$ where $q \in \{-1, 0, 1\}$ since movements must alternate in sign. Therefore,

$$\begin{aligned}
t - s &= c_{+1} \cdot d_{+1} + c_{-2} \cdot d_{-2} + c_{-3} \cdot d_{-3} \\
&= (c_{-2} + c_{-3} + q) \cdot d_{+1} + c_{-2} \cdot d_{-2} + c_{-3} \cdot d_{-3} \\
&= (c_{-2} + c_{-3} + q) \cdot (-1, 0) + c_{-2} \cdot (-1/2, -\sqrt{3}/2) + c_{-3} \cdot (-1/2, \sqrt{3}/2) \\
&= q \cdot (-1, 0) + c_{-2} \cdot (-3/2, -\sqrt{3}/2) + c_{-3} \cdot (-3/2, \sqrt{3}/2) \\
&= q \cdot (-1, 0) + c_{-2} \cdot (-3, 0) + (c_{-3} - c_{-2}) \cdot (-3/2, \sqrt{3}/2) \\
&= (3c_{-2} + q) \cdot (-1, 0) + (c_{-3} - c_{-2}) \cdot (-3/2, \sqrt{3}/2).
\end{aligned}$$

We now break the problem into two cases based on the sign of $3c_{-2} + q$.

Case 1: $3c_{-2} + q \geq 0$. This implies that t is in the cone emanating from s in the directions $(-1, 0)$ and $(-3/2, \sqrt{3}/2)$ as depicted in Fig. 25.

The directions $(-1, 0)$ and $(-3/2, \sqrt{3}/2)$ are adjacent in a 12-Hex grid graph. By Theorem 9, there is an s to t 12-Hex grid graph path that avoids all blocked hexagons and uses only the red, dashed movements in Fig. 26.

This 12-Hex grid path is easily converted into a 3-Hex grid path by replacing each segment as described in Fig. 26. Moreover, the resulting 3-Hex grid path avoids blocked hexagons since it traverses the same set of hexagons as the 12-Hex grid path. Finally, the resulting 3-Hex grid path is also an SGP; it only uses directions d_{+1}, d_{-2}, and d_{-3} and by Lemma 13, is an SGP when there are no blocked hexagons. Therefore it is also an SGP with the blocked hexagons since it avoids them, thereby completing case 1.

Case 2: $3c_{-2} + q < 0$. As such, $q = -1$ and $c_{-2} = 0$ implying $c_{-3} = c_1 + 1 \geq 1$. Therefore

$$\begin{aligned}
t - s &= (3c_{-2} + q) \cdot (-1, 0) + (c_{-3} - c_{-2}) \cdot (-3/2, \sqrt{3}/2) \\
&= (1, 0) + c_{-3} \cdot (-3/2, \sqrt{3}/2) \\
&= (-1/2, \sqrt{3}/2) + (c_{-3} - 1) \cdot (-3/2, \sqrt{3}/2)
\end{aligned}$$

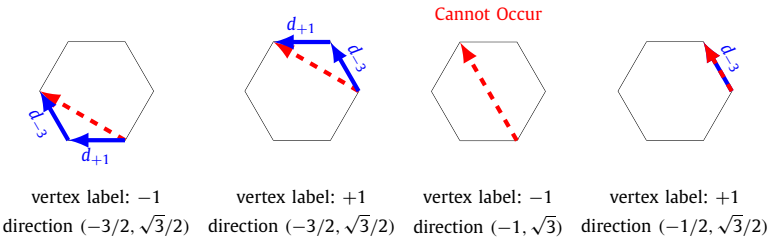

Fig. 27. Converting a 12-Hex grid path to a 3-Hex grid path (case 2).

and t is in the cone emanating from s in the directions $(-3/2, \sqrt{3}/2)$ and $d_{-3} = (-1/2, \sqrt{3}/2)$. The proof now follows almost identically to case 1. There directions are adjacent in a 12-Hex grid graph and there exists a 12-Hex grid graph from s to t using only the movements in Fig. 27.

Unlike case 1, only 3 of the 4 movements can occur. Since $(-1/2, \sqrt{3}/2)$ and $(-3/2, \sqrt{3}/2)$ are linearly independent, $t - s = a_1 \cdot (-1/2, \sqrt{3}/2) + a_2 \cdot (-3/2, \sqrt{3}/2)$ is uniquely expressed with the coefficients $a_1 = 1$ and $a_2 = c_{-3} - 1$. Thus, the movement $(-1, \sqrt{3})$ cannot occur as it would require $a_1 \geq 2$. As in case 1, a 3-Hex grid path can be constructed using the transformation described in Fig. 27 and will result in a SGP from s to t that avoids all blocked hexagons. Therefore, both cases have been proven and the statement of Theorem 14 holds. □

Theorem 15. *For 3-Hex grid graphs, the ratio between the SGP and TSP is at most $\frac{3}{2}$. Furthermore, if s and t have line of sight, then the worst-case ratio converges to $\frac{4}{3}$ as the length of the SGP tends to infinity.*

The theorem statements hold immediately from Theorems 1, 12, and 14.

6. Conclusions

In this article, we studied how much longer a shortest grid path can be than a corresponding true shortest path on all regular grids with blocked polygons that tessellate continuous 2D environments. We studied 5 different vertex connectivities that result from both different tessellations and different definitions of the neighbors of a vertex. Our analysis yielded either tight or asymptotically tight worst-case bounds in a unified framework. In our future work, we will study additional tessellations and definitions of the neighbors of a vertex, such as 16-Square and 9-Hex grid graphs.

Declaration of competing interest

The authors declare that they have no known competing financial interests or personal relationships that could have appeared to influence the work reported in this paper.

Acknowledgements

We thank K. Daniel, A. Felner, M. Likhachev, S. Sun, W. Yeoh and X. Zheng for their contributions to research that convinced us of the usefulness of this article. Our research has been supported by NSF under grant numbers CMMI-1335301, IIS-1319966, IIS-1409987, IIS-1724392, IIS-1817189, and IIS-1837779, ARO under grant number W911NF-08-1-0468, ONR under grant number N00014-09-1-1031, and Northrop Grumman via a fellowship to Alex Nash. The views and conclusions contained in this document are those of the authors and should not be interpreted as representing the official policies, either expressed or implied, of the sponsoring organizations, agencies, companies or the U.S. government.

Appendix A. Parallelogram grid property for 4-square, 8-square, 6-tri, and 12-hex

We first show the parallelogram grid property for the 4-Square grid graph. We then establish a new coordinate system for the other 3 grid graphs so that the proofs follow identically.

Proposition 16. *[Parallelogram Grid Graph for 4-Square] For any vertex t in the cone emanating from s in the adjacent directions d_1 and d_2, t can be reached from s using only the directions d_1 and d_2 when there are no blocked polygons.*

Proof. Recall $d_1 = (1, 0)$ and $d_2 = (0, 1)$. Without loss of generality, let $s = (0, 0)$. Every integer point, and therefore every vertex of an 4-grid graph, can be expressed as $t = c_1 \cdot d_1 + c_2 \cdot d_2$ for integers c_1 and c_2. As such, t is a vertex in the cone if and only if c_1 and c_2 are non-negative integers.

We proceed by induction on $k = c_1 + c_2$. The result trivially holds for $k = 0$ ($s = t$). We now show the result holds for $c_1 + c_2 = k + 1$.

Case 1: $c_2 \geq 1$. This implies that $t' = t - d_2 = c_1 \cdot d_1 + (c_2 - 1) \cdot d_2$ where $c_2 - 1 \geq 0$. Thus, t' is in the cone as well. Further, $c_1 + c_2 - 1 = k$ and, by induction, there is a path from s to t' using only d_1 and d_2 and s to t' to t describes a path from s to t using only directions d_1 and d_2.

Case 2: $c_2 = 0$ and therefore $c_1 \geq 1$ since $c_1 = k + 1 \geq 1$. By induction, $t' = t - d_1$ is reached from s using only directions d_1 and d_2 and there is a path from s to t' to t that uses only directions d_1 and d_2.

In both cases, the inductive step holds completing the proof of the proposition. □

Proposition 17. *[Parallelogram Grid Graph for 6-Tri] For any vertex t in the cone emanating from s in the adjacent directions d_1 and d_2, t can be reached from s using only the directions d_1 and d_2 when there are no blocked polygons.*

Proof. Without loss of generality, let $s = (0, 0)$. The point t is a vertex of a triangle if and only if $t = \sum_{i=1}^{6} c_i \cdot d_i$ for non-negative integers $c_1, ..., c_6$. We first claim that t is a vertex of a triangle if and only if $t = a_1 \cdot d_1 + a_2 \cdot d_2$ for integers $a_1, ..., a_2$.

($\Rightarrow$) Suppose t is a vertex and $t = \sum_{i=1}^{6} c_i \cdot d_i$ for non-negative integers $c_1, ..., c_6$. Then

$$\begin{aligned}
t &= \sum_{i=1}^{6} c_i \cdot d_i \\
&= \sum_{i=1}^{3} (c_i - c_{3+i}) \cdot d_i \\
&= (c_1 - c_4) \cdot (1, 0) + (c_2 - c_5) \cdot (1/2, \sqrt{3}/2) + (c_3 - c_6) \cdot (-1/2, \sqrt{3}/2) \\
&= (c_1 - c_4) \cdot (1, 0) + (c_2 - c_5) \cdot (1/2, \sqrt{3}/2) + (c_3 - c_6) \cdot \Big[(1/2, \sqrt{3}/2) - (1, 0)\Big] \\
&= (c_1 - c_4 - c_3 + c_6) \cdot (1, 0) + (c_2 - c_5 + c_3 - c_6) \cdot (1/2, \sqrt{3}/2) \\
&= (c_1 - c_4 - c_3 + c_6) \cdot d_1 + (c_2 - c_5 + c_3 - c_6) \cdot d_2
\end{aligned}$$

completing the first direction.

($\Leftarrow$) Suppose $t = a_1 \cdot d_1 + a_2 \cdot d_2$ for integer a_i. Let $a_i^+ \geq 0$ and $a_i^- \geq 0$ be integer and such that $a_i = a_i^+ - a_i^-$. Then $t = \sum_{i=1}^{2} a_i^+ \cdot d_i + \sum_{i=1}^{2} a_i^- \cdot (-d_i) = \sum_{i=1}^{2} a_i^+ \cdot d_i + \sum_{i=1}^{2} a_i^- \cdot d_{i+3}$ and t is a vertex.

The proof now follows identically to Proposition 16 using $t = a_1 \cdot d_1 + a_2 \cdot d_2$ for integers $a_1, ..., a_2$. □

Proposition 4 [Parallelogram Grid Graph for 8-Square]. For any vertex t in the cone emanating from s in the adjacent directions d_1 and d_2, t can be reached from s using only the directions d_1 and d_2 when there are no blocked polygons.

Proof. Without loss of generality, let $s = (0, 0)$. Following identically to the proof of Proposition of 17, t is a vertex if and only if $t = c_1 \cdot d_1 + c_2 \cdot d_2$ for some integers c_1, c_2. The proof now follows identically to Proposition 16. □

Proposition 18. *[Parallelogram Grid Graph for 12-Hex] For any vertex t in the cone emanating from s in the adjacent directions d_1 and d_2, t can be reached from s using only the directions d_1 and d_2 (and equivalent directions d_1' and d_2') when there are no blocked polygons.*

Proof. We begin by characterizing the set of vertices. First, observe that every vertex is either the lower left or lower right vertex of some hexagon so it suffices to characterize the lower left and lower right vertices of all hexagons. Let v be the lower left vertex of the hexagon H and therefore $v + d_1$ is the lower right vertex. Let $\bar{d} = 3 \cdot d_1 = (3, 0)$. The tessellation of hexagons is formed by shifting a hexagon by integer combinations of d_2 and $\bar{d}$. Thus, t is a vertex if and only if $t = v + c_1 \cdot d_1 + c_2 \cdot d_2 + \bar{c} \cdot \bar{d}$ for $c_1 \in \{0, 1\}$ and integers $c_2, \bar{c}$. Specifically, t is lower left vertex if $c_1 = 0$ and a lower right vertex if $c_1 = 1$.

Suppose that $s = (0, 0) = v + w \cdot d_1$ where $w \in \{0, 1\}$ depending on whether s is a lower left or lower right vertex. Then $t = (c_1 - w) \cdot d_1 + c_2 \cdot d_2 + \bar{c} \cdot \bar{d}$ is in the cone emanating from s in directions d_1 and d_2 if and only if $c_2 \geq 0$ and $c_1 - w + 3 \cdot \bar{c} \geq 0$.

We now proceed by induction on $k = c_1 - w + 2 \cdot c_2 + 3 \cdot \bar{c}$. For $k = 0$, $c_2 = \bar{c} = 0$ and $c_1 = w$ implying $s = t$ and the result holds. We remark that the result rightfully does not hold for $k = -1$ because this would imply $t = s - d_1$, which is not in the cone. We now show the result for $k + 1$.

Case 1: $c_2 \geq 1$. This implies $k + 1 = c_1 - w + 2 \cdot c_2 + 3 \cdot \bar{c} \geq 2$ since $c_1 - w + 3 \cdot \bar{c} \geq 0$. Then $t' = t - d_2 = (c_1 - w) \cdot d_1 + (c_2 - 1) \cdot d_2 + \bar{c} \cdot \bar{d}$ is in the cone emanating from s. Moreover, $c_1 - w + 2 \cdot (c_2 - 1) + 3 \cdot \bar{c} = k - 1 \geq 0$ and, by strong induction, there is a grid path from s to t' to $t = t' + d_2$ using only the directions in the statement of the proposition.

Case 2: $c_2 = 0$ and $c_1 = 0$ (t is a left vertex). Therefore $k + 1 = -w + 3 \cdot \bar{c}$ implying $\bar{c} \geq 1$ and $k + 1 \geq 2$. Since t is a lower left vertex, $t - (2, 0) = t - d_2'$ is a lower right vertex. Moreover, $t' = t - d_2' = -w \cdot d_1 + \bar{c} \cdot \bar{d} - d_2' = (1 - w) \cdot d_1 + (\bar{c} - 1) \cdot \bar{d}$ is

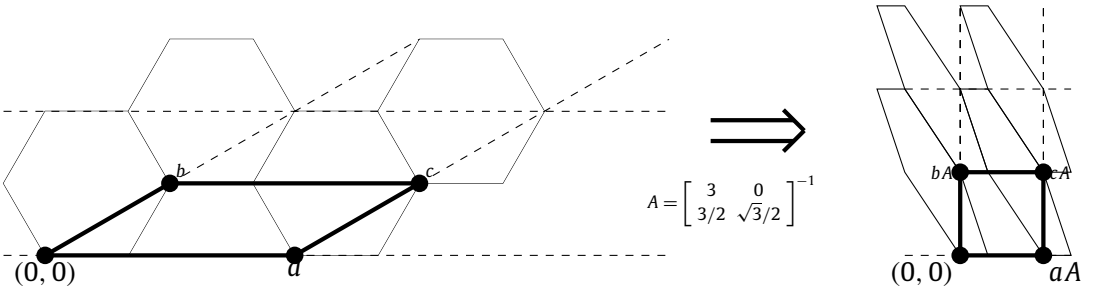

Fig. A.28. New basis defined by direction $d_2 = (1/2, \sqrt{3}/2)$ and $\bar{d} = (3, 0)$.

in the cone emanating from s. Further, $(1 - w) + 3 \cdot (\bar{c} - 1) = k - 1 \geq 0$ and, by strong induction, there is a grid path from s to t' to $t = t' + d_2'$ using only the directions in the statement of the proposition.

Case 3: $c_2 = 0$ and $c_1 = 1$ (t is a right vertex). Therefore $-w + 3 \cdot \bar{c} \geq 0$ since $k + 1 = 1 - w + 3 \cdot \bar{c}$. Since t is a right vertex, $t' = t - (1, 0) = t - d_1$ is a left vertex. Moreover, $t' = t - d_1 = -w \cdot + \bar{c} \cdot \bar{d}$ is in the cone emanating from s. Thus, by induction, there is a path from s to t' to $t = t + d_1$ using only the directions in the statement of the proposition.

In all three cases, the inductive step holds completing the proof of the proposition. □

We remark that this characterization of vertices is consistent with the transformation in Section 4 and shown in Fig. A.28. In particular, after the transformation A to a new basis, the vertex t is expressed as $tA = (v + c_1 \cdot d_1 + c_2 \cdot d_2 + \bar{c} \cdot \bar{d})A = vA + c_1 \cdot (1/3, 0) + c_2 \cdot (0, 1) + \bar{c} \cdot (1, 0)$. Assuming vertex $v = (0, 0)$ is in the lower left corner of a hexagon, each vertex has rational coordinates – a multiple of $1/3$ – in the new space. Moreover, the integer points in the transformed space precisely describe the coordinates of vertices in the lower left corners of hexagons.

References

[1] M. Martin, H. Moravec, Robot evidence grids, Tech. Rep. CMU-RI-TR-96-06, Carnegie Mellon University, 1996.
[2] J. Carsten, A. Rankin, D. Ferguson, A. Stentz, Global planning on the Mars exploration rovers: software integration and surface testing, J. Field Robot. 26 (4) (2009) 337–357, https://doi.org/10.1002/rob.v26:4.
[3] Y. Björnsson, M. Enzenberger, R. Holte, J. Schaeffer, P. Yap, Comparison of different grid abstractions for pathfinding on maps, in: Proceedings of the International Joint Conference on Artificial Intelligence, 2003, pp. 1511–1512.
[4] H. García, L. Garrido, Towards exploration of unknown dynamic worlds using multiple robots, in: Proceedings of the Mexican International Conference on Artificial Intelligence, 2007, pp. 407–417.
[5] P. Yap, Grid-based path-finding, in: Proceedings of the Canadian Conference on Artificial Intelligence, 2002, pp. 44–55.
[6] P. Tozour, Search space representations, in: S. Rabin (Ed.), AI Game Programming Wisdom 2, Charles River Media, 2004, pp. 85–102.
[7] D. Lee, Proximity and reachability in the plane, Ph.D. thesis, University of Illinois at Urbana-Champaign, 1978.
[8] T. Lozano-Pérez, M. Wesley, An algorithm for planning collision-free paths among polyhedral obstacles, Commun. ACM 22 (1979) 560–570.
[9] A. Nash, Any-angle path planning, Ph.D. thesis, University of Southern California, 2012.
[10] P. Chew, There is a planar graph almost as good as the complete graph, in: Proceedings of the Annual Symposium on Computational Geometry, 1986, pp. 205–219.
[11] D.P. Dobkin, S.J. Friedman, K.J. Supowit, Delaunay graphs are almost as good as complete graphs, in: Proceedings of the Annual Symposium on Foundations of Computer Science, 1987, pp. 20–26.
[12] P.C. Hew, The length of shortest vertex paths in binary occupancy grids compared to shortest r-constrained ones, J. Artif. Intell. Res. 59 (2017) 543–563.
[13] B. Kramm, N. Rivera, C. Hernandez, J.A. Baier, A suboptimality bound for 2^k grid path planning, in: Eleventh Annual Symposium on Combinatorial Search, 2018, pp. 63–71.
[14] A. Nash, S. Koenig, Any-angle path planning, AI Mag. 34 (4) (2013) 85–107.
[15] P. Hart, N. Nilsson, B. Raphael, A formal basis for the heuristic determination of minimum cost paths, IEEE Trans. Syst. Sci. Cybern. 4 (1968) 100–107.
[16] D. Harabor, A. Grastien, An optimal any-angle pathfinding algorithm, in: Proceedings of the International Conference on Automated Planning and Scheduling, 2013, pp. 308–311.
[17] P. Yap, N. Burch, R. Holte, J. Schaeffer, Any-angle path planning for computer games, in: Proceedings Conference on Artificial Intelligence and Interactive Digital Entertainment, 2011, pp. 201–207.
[18] A. Nash, S. Koenig, Theta* for any-angle path finding, in: S. Rabin (Ed.), Game AI Pro 2: Collected Wisdom of Game AI Professionals, A K Peters/CRC, 2015, pp. 161–171.
[19] D. Harabor, A. Grastien, D. Öz, V. Aksakalli, Optimal any-angle pathfinding in practice, J. Artif. Intell. Res. 56 (2016) 89–118.
[20] P. Yap, N. Burch, R. Holte, J. Schaeffer, Block A*: database-driven search with applications in any-angle path-planning, in: Proceedings of the AAAI Conference on Artificial Intelligence, 2011, pp. 120–125.
[21] A. Nash, S. Koenig, Theta* for any-angle pathfinding, in: Game AI Pro 360, CRC Press, 2019, pp. 125–136.
[22] A. Nash, S. Koenig, Any-angle path planning, AI Mag. 34 (4) (2013) 85–107.
[23] D. Ferguson, 2013, Personal communication.
[24] C. Petres, Y. Pailhas, P. Patron, Y. Petillot, J. Evans, D. Lane, Path planning for autonomous underwater vehicles, IEEE Trans. Robot. 23 (2) (2007) 331–341.
[25] D. Šišlák, P. Volf, M. Pěchouček, Accelerated A* path planning, in: Proceedings of the International Joint Conference on Autonomous Agents and Multiagent Systems, 2009, pp. 1133–1134.
[26] D. Šišlák, P. Volf, M. Pěchouček, Accelerated A* trajectory planning: grid-based path planning comparison, in: Proceedings of the Workshop on Planning and Plan Execution for Real-World Systems at the International Conference on Automated Planning and Scheduling, 2009, pp. 74–81.
[27] R.M. Avjian, J. Dehn, Trajectory-based integration of aircraft conflict detection and weather avoidance fields, in: Proceedings of the American Meteorological Society Annual Meeting: Third Aviation, Range and Aerospace Meteorology Special Symposium on Weather-Air Traffic Management Integration, 2012.

[28] M. Garcia, A. Viguria, A. Ollero, Dynamic graph-search algorithm for global path planning in presence of hazardous weather, J. Intell. Robot. Syst. 69 (1–4) (2013) 285–295.
[29] D. Ferguson, A. Stentz, Using interpolation to improve path planning: the Field D* algorithm, J. Field Robot. 23 (2) (2006) 79–101.
[30] J. Carsten, D. Ferguson, A. Stentz, 3D Field D*: improved path planning and replanning in three dimensions, in: Proceedings of the IEEE International Conference on Intelligent Robots and Systems, 2006, pp. 3381–3386.
[31] L. Sapronov, A. Lacaze, Path planning for robotic vehicles using Generalized Field D*, in: Proceedings of the SPIE: Unmanned Systems Technology X, vol. 6962, 2008, pp. 69621C–69621C–12.
[32] S. Perkins, P. Marais, J. Gain, M. Berman, Field D* path-finding on weighted triangulated and tetrahedral meshes, Auton. Agents Multi-Agent Syst. 26 (3) (2012) 354–388.
[33] A. Nash, K. Daniel, S. Koenig, A. Felner, Theta*: any-angle path planning on grids, in: Proceedings of the AAAI Conference on Artificial Intelligence, 2007, pp. 1177–1183.
[34] A. Nash, S. Koenig, C. Tovey, Lazy Theta*: Any-angle path planning and path length analysis in 3D, in: Proceedings of the AAAI Conference on Artificial Intelligence, 2010, pp. 147–154.
[35] J. Bailey, C. Tovey, T. Uras, S. Koenig, A. Nash, Path planning on grids: the effect of vertex placement on path length, in: Proceedings of the Conference on Artificial Intelligence and Interactive Digital Entertainment, 2015, pp. 108–114.
[36] B. Nagy, Shortest paths in triangular grids with neighbourhood sequences, CIT, J. Comput. Inf. Technol. 11 (2) (2003) 111–122.
[37] A.J. Kempner, A theorem on lattice-points, Ann. Math. 19 (2) (1917) 127–136.